Andreev bound states and self-consistent gap functions in clean layered superconductor/normal metal systems with finite transverse width

Lodder, A.; Otadoy, R. E. S.

published in
Physical Review B. Condensed Matter and Materials Physics
2001

document version
Publisher's PDF, also known as Version of record

Andreev bound states and self-consistent gap functions in clean layered superconductor/normal metal systems with finite transverse width

R. E. S. Otadoy* and A. Lodder†
Faculty of Sciences/Natuurkunde en Sterrenkunde, Vrije Universiteit De Boelelaan 1081, 1081 HV Amsterdam, The Netherlands
(Received 14 March 2001; revised manuscript received 23 May 2001; published 19 December 2001)

Andreev bound states in clean, ballistic *SNS* and *SNSNS* junctions are calculated exactly and by using the Andreev approximation (AA). The AA appears to break down for junctions with transverse dimensions chosen such that the motion in the longitudinal direction is very slow. The doubly degenerate states typical for the traveling waves found in the AA are replaced by two standing waves in the exact treatment and the degeneracy is lifted. A multiple-scattering Green's function formalism is used, from which the states are found through the local density of states. The scattering by the interfaces in any layered system of ballistic normal metals and clean superconducting materials is taken into account exactly. The formalism allows, in addition, for a self-consistent determination of the gap function. In the numerical calculations the pairing coupling constant for aluminum is used. Various features of the proximity effect are shown.

DOI: 10.1103/PhysRevB.65.024521 PACS number(s): 74.80.Dm

I. INTRODUCTION

Andreev bound states[1] occur in a normal metal (*N*) system of finite size that is in contact with superconductors (*S*). Although much is known already about these states, still new features are measured by varying the length of the normal metal,[2,3] by looking at phenomena induced by introducing a constriction in the normal part,[4] or by studying questions such as the occurrence of a ''minigap.''[5,6] All these developments are induced by phenomena which show up only in smaller and smaller, mesoscopic samples.[7] In quite some studies the samples can still be described in the dirty limit,[8] in others the clean, ballistic limit is most appropriate regarding the phenomena involved.[6,9,10] In almost all studies mentioned a quasiclassical description is used,[11] which for the clean limit has been proven to be equivalent to the Andreev approximation.[1,10] In the Andreev approximation (AA) normal reflection of an electron approaching an *NS* interface is neglected and only the Andreev type reflection, implying just a reflected hole retracing the path of the incident electron, is accounted for. Interestingly, in many cases the AA works remarkably well, implying negligible effects of less than 0.1%.[12]

In the present paper we address *transverse* size effects in a situation where neither the quasiclassical approach nor the Andreev approximation can help, and we have to proceed with an exact calculation. In many studies the systems are treated as being infinite in the transverse directions, by which breakdown of the AA hardly can show up.[13–15] Kümmel[16] was the first who pointed out that for an electron moving slowly in the direction of an *NS* interface, so having a relatively large transverse momentum, the Andreev approximation breaks down. At the interface not only a returning hole amplitude is generated, but also a not negligible electron amplitude is reflected. While Kümmel worked out this idea for a superconducting layer with a thickness comparable to the superconducting coherence length, Šipr and Györffy[17] first have shown explicitly its dramatic impact for a standard *SNS* junction. For these effects an exact calculation is required, going beyond the quasiclassical approach. In fact, exact calculations are becoming more and more important, either in the form of solving the Bogoliubov equations exactly,[17] by using a scattering matrix formalism,[4] or by using the exact Green's function as it is done in the present paper.[18]

We use the work of Tanaka and Tsukada as a starting point.[13] These authors investigated the energy spectrum of the quasiparticle states in a superconducting superlattice based on a Kronig-Penney model potential. Their calculations were done using the Andreev approximation and the system considered was infinite in both the transverse and the longitudinal dimensions. We will deal with three additional aspects: (i) we do the exact calculation and investigate the reliability of the Andreev approximation, (ii) we do the calculation for a limited number of layers, which relates better to a possible experimental situation, and (iii) we investigate the transverse size dependence of the relevant properties such as the local density of states. The systems we consider cover the entire range from very narrow transverse dimensions to wider ones, thereby simulating one, two, and three-dimensional systems.

The multiple-scattering Green's function formalism to be used[18] is an extension of the formalism introduced by Tanaka and Tsukada[13] in that no Andreev approximation is made. In addition it is set up in a quite different way, such that the multiple scattering of the (quasi)particles by the different interfaces is exhibited explicitly. The formalism is very flexible, in that an arbitrary number of layers can be accounted for in a transparent way, supercurrents can be calculated and the gap function can be determined self-consistently. In an initial application of the theory the local density of states of normal metal-superconductor (*NS*) and *SNS* junctions were calculated, but the breakdown of the Andreev approximation was not noticed.[12]

The paper is organized as follows. First we give a concise account of the main features of the theory. In Sec. III the local density of states for the two systems considered is studied. In Sec. IV the gap function is calculated self-consistently for a bar-shaped superconductor and for the *NS*, *SNS*, and

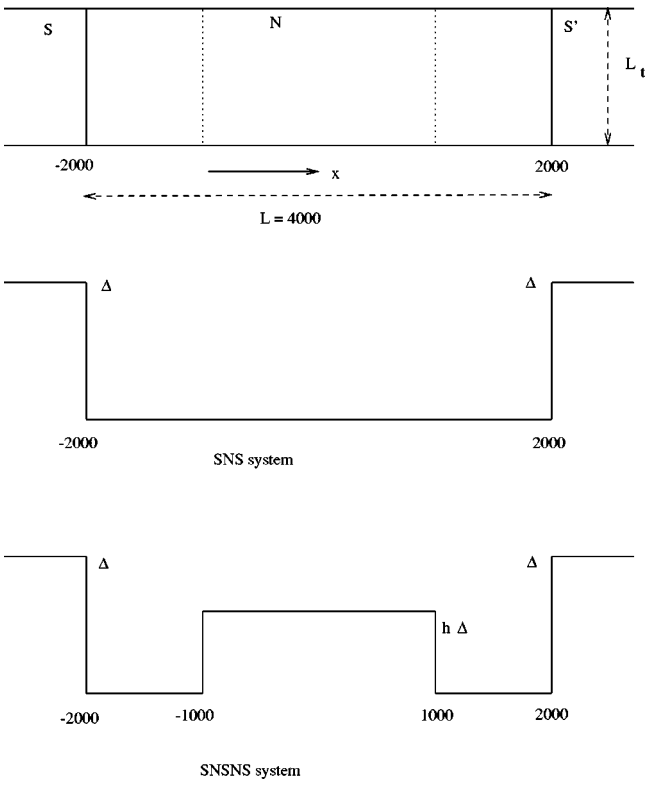

FIG. 1. A two-dimensional picture of the systems studied. In the upper panel the vertical direction stands for a transverse direction. In the lower panels the potential is shown, which is zero in the normal part(s), and proportional to Δ in the superconducting parts.

SNSNS junctions. Concluding remarks are given in Sec. V. Throughout the paper, Rydberg atomic units are used, in which the energy is in Rydberg, the distance is in Bohr ($1\ \text{Bohr}\approx 0.5\ \text{Å}$), $\hbar=1$, and the electronic mass is $\frac{1}{2}$.

II. THEORY

Although in this paper a Green's function formalism is used, we first give the Bogoliubov–de Gennes equations

$$\begin{bmatrix} -\nabla^2-\mu & \Delta(\mathbf{r}) \\ \Delta^*(\mathbf{r}) & \nabla^2+\mu \end{bmatrix}\Psi(\mathbf{r})=E\Psi(\mathbf{r})\equiv E\begin{pmatrix} u(\mathbf{r}) \\ v(\mathbf{r}) \end{pmatrix} \tag{1}$$

used by Šipr and Györffy[17] to investigate the bound states of a *SNS* junction shown in the upper panels of Fig. 1. The main reason is that our formalism will be expressed in terms of the solutions of these equations. The inhomogeneity of the system is expressed by the space dependence of the gap $\Delta(\mathbf{r})$. In the superconducting parts the gap is a complex constant whereas in the normal metal it is zero. The spinor wave function describes quasiparticle excitations and the energy E is measured with respect to the Fermi energy μ.

Application of the Bogoliubov–de Gennes equations to the bar-shaped superconductor shown in Fig. 2 yields

$$\Psi(\mathbf{r})=\begin{pmatrix} u_S^{\sigma}e^{i\phi/2} \\ u_S^{-\sigma}e^{-i\phi/2} \end{pmatrix} e^{i\sigma\nu k_S^{\sigma}x}\sin\left(\frac{n_y\pi}{L_y}y\right)\sin\left(\frac{n_z\pi}{L_z}z\right), \tag{2}$$

where ϕ is the phase of the complex constant Δ, and

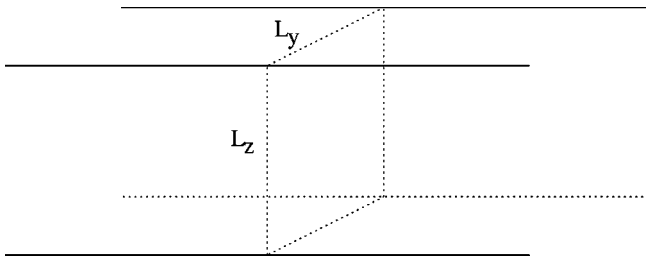

FIG. 2. The geometry of the bar-shaped superconductor under consideration. It has finite transverse dimension and is infinite longitudinally. A rectangular cross section is shown whose dimensions are L_y and L_z.

$$k_y=\frac{n_y\pi}{L_y};\quad k_z=\frac{n_z\pi}{L_z},\quad \text{with}\ \ n_y,n_z=1,2,3,..., \tag{3}$$

$$u_S^{\sigma}=\sqrt{E+\sigma\sqrt{E^2-|\Delta|^2}}, \tag{4}$$

$$k_S^{\sigma}=\sqrt{k_{F_x}^2+\sigma\sqrt{E^2-|\Delta|^2}}, \tag{5}$$

$$k_{F_x}^2=\mu-k_y^2-k_z^2. \tag{6}$$

The discretized nature of the transverse wavevectors is due to the vanishing of the wave functions on the transverse boundaries. The four standard solutions are labeled with the sign indices σ and ν that can both be equal to ± 1. By this convention, the index σ refers to the type of particle (electronlike for $\sigma=+1$ and holelike for $\sigma=-1$) and the index ν indicates the direction of propagation ($\nu=+1$ to the right and $\nu=-1$ to the left). The complete solution of Eq. (1) is a linear superposition of Eq. (2) for different possible combinations of (σ, ν). The above equations also hold for a normal metal by letting $\Delta=0$, in which case the subscript S is to be replaced by N.

The Green's function formalism is outlined extensively by Koperdraad *et al.*[18] It is an extension of the microscopic theory used by Tanaka and Tsukada, in that the electron-hole scattering properties are treated exactly, and it traces back to the microscopic description of superconductivity by Gor'kov[19] and Ishii.[20] For the sake of completeness and clarity we summarize its main features and add relevant new elaborations. The matrix Green's function satisfies the equation

$$\begin{bmatrix} i\omega_n+\nabla^2+\mu & -\Delta(\mathbf{r}) \\ -\Delta^*(\mathbf{r}) & i\omega_n-\nabla^2-\mu \end{bmatrix} G(\mathbf{r},\mathbf{r}',i\omega_n)=\delta(\mathbf{r}-\mathbf{r}')\mathbf{1} \tag{7}$$

in which the differential operator is closely related to the operator in the Bogoliubov–de Gennes equations (1) apart from the replacement of E by $i\omega_n$, where

$$\omega_n=\pi n k_B T\ \ \text{with}\ \ n\ \ a\pm\text{odd integer}. \tag{8}$$

The quantity ω_n is called the Matsubara frequency. Possible inhomogeneities of the system are fully represented by the $\mathbf{r}$ dependence of the gap function. As far as the transverse directions are concerned the general solution of Eq. (7) can be

expressed as a linear combination of solutions (2) over all allowed values of k_y, k_y', k_z, and k_z'. Thus

$$G(\mathbf{r},\mathbf{r}',i\omega_n)=\frac{4}{L_yL_z}\sum_{k_y,k_y',k_z,k_z'} G(x,x',k_y,k_y',k_z,k_z',i\omega_n) \times \sin k_y y \sin k_y' y' \sin k_z z \sin k_z' z'. \tag{9}$$

The transverse standing waves are normalized to unity, which implies the orthogonality condition

$$\int_0^{L_y} \sin k_y y \sin \overline{k_y} y dy = \frac{L_y}{2}\delta_{k_y,\overline{k_y}}, \tag{10}$$

for the y coordinate and a similar condition for the z coordinate. The Fourier coefficient $G(x,x',k_y,k_y',k_z,k_z',i\omega_n)$ can be obtained from Eq. (9) using Eq. (10). It takes the form

$$\begin{aligned} &G(x,x',k_y,k_y',k_z,k_z',i\omega_n) \\ &\quad=\frac{4}{L_yL_z}\int_0^{L_y}\sin k_y y\int_0^{L_y}\sin k_y' y'\int_0^{L_z}\sin k_z z \\ &\qquad\times\int_0^{L_z}\sin k_z' z' G(\mathbf{r},\mathbf{r}',i\omega_n)dz'dzdy'dy. \end{aligned} \tag{11}$$

Using Eq. (11), Eq. (7) can be written as

$$\begin{aligned} &\begin{bmatrix} i\omega_n+\dfrac{d^2}{dx^2}+k_{F_x}^2 & -\Delta \\ -\Delta^* & i\omega_n-\dfrac{d^2}{dx^2}-k_{F_x}^2 \end{bmatrix} \\ &\qquad\times G(x,x',k_y,k_y',k_z,k_z',i\omega_n) \\ &\quad=\delta(x-x')\delta_{k_y,k_y'}\delta_{k_z,k_z'}\mathbf{1}. \end{aligned} \tag{12}$$

Before we proceed we want to make the terminology clear. $G(\mathbf{r},\mathbf{r}',i\omega_n)$ is the actual Green's function. The Fourier coefficient $G(x,x',k_y,k_y',k_z,k_z',i\omega_n)$ is a Green's function in the sense that it is the solution of Eq. (12), but this equation demonstrates that it is diagonal in k_y and k_z. That facilitates both the notation, because the variables k_y' and k_z' can be omitted, and the calculation of $G(\mathbf{r},\mathbf{r}',i\omega_n)$ according to Eq. (9). In calculating the local density of states and the self-consistent gap function, we will need the Green's function for diagonal spatial coordinates. As long as we keep $x\neq x'$, we can already take $y=y'$ and $z=z'$ in Eq. (9). Since we are only interested in the variations over the longitudinal direction x, we can average over the transverse dimensions. By that Eq. (9) simplifies to the series

$$G(x,x',i\omega_n)=\frac{1}{L_yL_z}\sum_{k_y,k_z} G(x,x',k_y,k_z,i\omega_n). \tag{13}$$

First we give the Green's function of a homogeneous bar-shaped superconductor

$$\begin{aligned} G_S^0(x,x',k_y,k_z,i\omega_n)&=\sum_\sigma d_S^\sigma \psi_S^{\sigma-}(x_<)\tilde{\psi}_S^{\sigma+}(x_>) \\ &=\sum_\sigma d_S^\sigma \psi_S^{\sigma+}(x_>)\tilde{\psi}_S^{\sigma-}(x_<), \\ &\text{with}\quad d_S^\sigma=-\frac{1}{4\Omega_S k_S^\sigma}, \end{aligned} \tag{14}$$

in which $i\Omega_S=\sqrt{(i\omega_n)^2-|\Delta|^2}$. The wave function $\psi_S^{\sigma\nu}(x)$ is given by Eq. (2) after omitting the transverse solutions, and u_S^σ and k_S^σ are given by Eqs. (4) and (5) with the replacement $E\to i\omega_n$. In addition the conjugate wave function is defined by

$$\tilde{\psi}_S^{\sigma\nu}(x)=(u_S^\sigma e^{-i\phi/2}u_S^{-\sigma}e^{i\phi/2})e^{i\sigma\nu k_S^\sigma x}. \tag{15}$$

The Green's function (14) describes the propagation of excitations (holelike or electronlike) from the starting point x' to the final point x with the weighting factor d_S^σ. In this case of a superconducting bar, there is no scattering.

Now we give the Green's function for a system with one interface. To account for the scattering at the interface, its appropriate form appears to be[21]

$$\begin{aligned} &G_{\nu j\nu' j}(x,x',k_y,k_z,i\omega_n) \\ &\quad=G_{\nu j}^0(x,x',k_y,k_z,i\omega_n)\delta_{\nu\nu'} \\ &\qquad+\sum_{\sigma\sigma'} d_{\nu j}^\sigma d_{\nu' j}^{\sigma'}\psi_{\nu j}^{\sigma\nu}(x)t_{\nu j\nu' j}^{\sigma\sigma'\nu\nu'}\tilde{\psi}_{\nu' j}^{\sigma'\nu'}(x'), \end{aligned} \tag{16}$$

where $G_{\nu j}^0$ is equal to G_S^0 given by Eq. (14), but for the present purpose rewritten as

$$\begin{aligned} &G_{\nu j}^0(x,x',k_y,k_z,i\omega_n) \\ &\quad=\sum_\sigma d_{\nu j}^\sigma \psi_{\nu j}^{\sigma\mu}(x)\tilde{\psi}_{\nu j}^{\sigma,-\mu}(x') \quad\text{with}\quad \mu=\mathrm{sgn}(x-x'). \end{aligned} \tag{17}$$

The label S in Eq. (14) has been replaced with the more flexible label νj indicating the position x_j of the interface. The subscript $+j$ means x is in the right-hand side of the interface x_j and $-j$ means that it is in the left-hand side. The first term is nonzero only if the starting and final points x' and x, respectively, are at the same side of the interface. The second term takes into account the scattering of the particle at the interface. This scattering is aptly described by the parameter we call scattering t matrix, $t_{\nu j\nu' j}^{\sigma\sigma'\nu\nu'}$. For a superconducting bar the t matrix is zero, because there is pure propagation and no scattering. The scattering t matrix can be obtained by imposing the continuity of the Green's function and its derivative at the interface. We then obtain

$$\sum_{\sigma\nu}\nu d_{\nu j}^\sigma \psi_{\nu j}^{\sigma\nu}(x_j)t_{\nu j\nu' j}^{\sigma\sigma'\nu\nu'}=-\nu'\psi_{\nu' j}^{\sigma',-\nu'}(x_j). \tag{18}$$

In applying the above interface matching condition, it has come out to be convenient to use an extended definition

$$\psi_S^{\sigma\nu}(x)=\begin{pmatrix} u_S^{\sigma}e^{i\phi/2} \\ u_S^{-\sigma}e^{-i\phi/2} \\ i\sigma\nu k_S^{\sigma}u_S^{\sigma}e^{i\phi/2} \\ i\sigma\nu k_S^{\sigma}u_S^{-\sigma}e^{-i\phi/2} \end{pmatrix} e^{i\sigma\nu k_S^{\sigma}x} \tag{19}$$

of the wave function $\psi_S^{\sigma\nu}(x)$ which includes the derivative with respect to x.

If there are more interfaces as in the systems depicted in Fig. 1, multiple scattering occurs and the Green's function is given by

$$G_{\nu j\nu' j'}(x,x',k_y,k_z,i\omega_n) = G^0_{\nu j}(x,x',k_y,k_z,i\omega_n)(\delta_{\nu\nu'}\delta_{jj'}+\delta_{-\nu\nu'}\delta_{j+\nu,j'}) + \sum_{\sigma\mu\sigma'\mu'} d^{\sigma}_{\nu j}d^{\sigma'}_{\nu' j'}\psi^{\sigma\mu}_{\nu j}(x)T^{\sigma\sigma'\mu\mu'}_{\nu j\nu' j'}\tilde{\psi}^{\sigma'\mu'}_{\nu' j'}(x'). \tag{20}$$

This is the generalization of Eq. (16). There are features in Eq. (20) that do not appear in that equation. One of these features is the strange combination of Kronecker deltas in the first term. The first set of Kronecker deltas $\delta_{\nu\nu'}\delta_{jj'}$ insures that the first term is nonzero only if the starting and final positions are in the same layer. The other set $\delta_{-\nu\nu'}\delta_{j+\nu,j'}$ serves the same purpose but at the same time it takes care of the redundancy in the indexing of the layers. The structure of the two sets of Kronecker deltas assures us that there is no overlapping of their functions. If one set gives the value unity the other set must be zero and vice versa. Another feature of Eq. (20) is the presence of the quantity $T^{\sigma\sigma'\mu\mu'}_{\nu j\nu' j'}$. Whereas the t matrix describes the scattering of the particle at a particular interface, this quantity describes the multiple scattering of the particle at the interfaces along its path. We call this the multiple scattering T matrix. The T matrix is in fact a function of the t matrix and is given by the multiple scattering equation

$$T^{\sigma\sigma'\nu\mu'}_{\nu j\nu' j'} = t^{\sigma\sigma'\nu\mu'}_{\nu j\mu' j'}(\delta_{\mu'\nu'}\delta_{jj'}+\delta_{-\mu',\nu'}\delta_{j+\mu',j'}) + \sum_{\sigma''\nu''} t^{\sigma\sigma''\nu\nu''}_{\nu j\nu'' j} d^{\sigma''}_{\nu'' j}T^{\sigma''\sigma',-\nu''\mu'}_{\nu'' j\nu' j'}. \tag{21}$$

To solve this equation it is necessary to first solve for the t-matrix at each interface using Eq. (18).

Until now no approximations have been made in using the solutions (2) of the Bogoliubov–de Gennes equations. In applying the formalism given above to the calculation of the density of states, $i\omega_n$ has to be replaced by $E+i\delta$. After that one can make the frequently used Andreev approximation, which amounts to the replacement

$$k^{\sigma}_{\nu j}\to k_{F_x}+\sigma\frac{\sqrt{E^2-|\Delta|^2}}{2k_{F_x}} \tag{22}$$

if $k^{\sigma}_{\nu j}$ occurs in the exponential and to $k^{\sigma}_{\nu j}\to k_{F_x}$ if $k^{\sigma}_{\nu j}$ occurs as a factor as shown explicitly in the third and fourth components of the wave function (19). This approximation is valid when E, $|\Delta|\ll k^2_{F_x}$. In the present paper we will investigate its limitation by looking at configurations in which E, $\Delta\approx k^2_{F_x}$.

III. THE LOCAL DENSITY OF STATES

Section II provides the basic machinery to determine the matrix Green's function, which enables us to calculate the local density of states (LDOS) at a position x using the equation

$$\mathrm{LDOS}(x,E)=-\frac{1}{\pi L_y L_z}\lim_{\delta\to 0}\sum_{k_y,k_z}\mathrm{Im}\,G_{11}(x,x;k_y,k_z,E+i\delta) \tag{23}$$

in which G_{11} is the upper left matrix element of the multiple scattering Green's function (20). Although we only study Andreev bound states, which imply infinite peaks at the bound-state energies, the Green's function formalism makes it possible to broaden the peaks by using a small value of δ. The peaks acquire a finite height and must correspond to the bound-state energies.

A. The *SNS* junction

We first apply the formalism discussed in Sec. II to a superconductor-normal metal-superconductor (*SNS*) junction. A schematic diagram of the system studied is given in the upper and middle panels of Fig. 1. The dotted lines in the upper panel serve as an indication of the position of the inner *NS* and *SN* interfaces in the *SNSNS* system to be treated in Sec. III B. In this first application we will show more explicitly how the different labels are used. The interface index j has only two values 1 and 2. The T-matrix equation (21) can be recast into the form

$$T^{-\sigma\sigma'-\nu\nu'}_{-\nu j\nu' j'} = t^{\sigma\sigma'-\nu\nu'}_{-\nu j\nu' j'}\delta_{jj'}+\sum_{\sigma''\nu''} t^{\sigma\sigma'-\nu\nu'}_{-\nu j\nu'' j'} d^{\sigma''}_{\nu'' j}T^{\sigma''\sigma',-\nu''\nu'}_{-\nu'',j+\nu'',\nu' j'}. \tag{24}$$

To implement this in matrix form, we must see to it that the elements of the T matrix in both sides of the equation are arranged in the same manner. Thus, its elements in the right-hand side of the equation must be similarly displayed as in the left-hand side. This can be done by writing Eq. (24) in the form

$$\begin{bmatrix} T^{\sigma\sigma'-\nu\nu'}_{-\nu 1\nu' 1} & T^{\sigma\sigma'-\nu\nu'}_{-\nu 1\nu' 2} \\ T^{\sigma\sigma'-\nu\nu'}_{-\nu 2\nu' 1} & T^{\sigma\sigma'-\nu\nu'}_{-\nu 2\nu' 2} \end{bmatrix} = \begin{bmatrix} t^{\sigma\sigma'-\nu\nu'}_{-\nu 1\nu' 1} & 0 \\ 0 & t^{\sigma\sigma'-\nu\nu'}_{-\nu 2\nu' 2} \end{bmatrix} + \begin{bmatrix} 0 & t^{\sigma\sigma''-\nu\nu''}_{-\nu 1\nu'' 1} d^{\sigma''}_{\nu'' 1}\delta_{\nu''+} \\ t^{\sigma\sigma''-\nu\nu''}_{-\nu 2\nu'' 2} d^{\sigma''}_{\nu'' 2}\delta_{\nu''-} & 0 \end{bmatrix} \times \begin{bmatrix} T^{\sigma\sigma''-\nu\nu''}_{-\nu 1\nu'' 1} & T^{\sigma\sigma''-\nu\nu''}_{-\nu 1\nu'' 2} \\ T^{\sigma\sigma''-\nu\nu''}_{-\nu 2\nu'' 1} & T^{\sigma\sigma''-\nu\nu''}_{-\nu 2\nu'' 2} \end{bmatrix}. \tag{25}$$

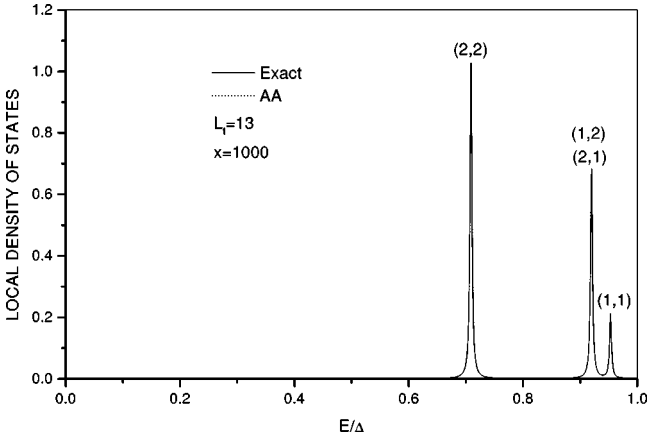

FIG. 3. Plot of the LDOS against E/Δ for a *SNS* system in which $L_t = 13$ Bohr.

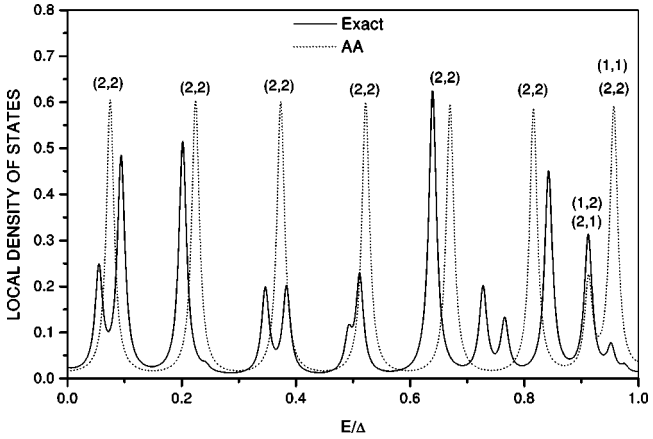

FIG. 4. Plot of the LDOS against E/Δ for $x = 1000$ Bohr, $L_t = 12.5676$ Bohr, $L = 4000$ Bohr, and $\Delta = 0.0001$ Ry.

Each element of the above matrices is itself a 4×4 matrix with $\sigma\nu$ $(=++, +-, -+, --)$ as row and column indices. So actually, the matrices appearing in Eq. (25) have dimensions 8×8. In this form the T matrix can be obtained by appropriate matrix inversion. The Green's function is obtained using Eq. (20). The local density of states is determined by using Eq. (23).

To investigate the validity of the Andreev approximation in our *SNS* junction, we will focus on the choice of the transverse width $L_y = L_z = L_t$ of the junctions. The transverse wave components of the wave function (2) are standing waves proportional to $\sin(k_y y)\sin(k_z z)$ where k_y and k_z are given by Eq. (3). The different combinations of (k_y, k_z) or (n_y, n_z) are called modes whose allowed values are determined by

$$k_{F_x}^2 = \mu - \left(\frac{\pi}{L_t}\right)^2 (n_y^2 + n_z^2) > 0. \tag{26}$$

When the transverse dimension is small, the second term in the right becomes large, as a result, only a few modes will be allowed. If this term exceeds the chemical potential μ, k_{F_x} becomes imaginary, the wavefunction is damped, and consequently, such mode cannot exist. For larger transverse dimensions, the second term is smaller whereupon more modes are allowed. Most of our calculations are done for small L_t so that only few modes will exist. By that the effects to be illustrated come out most clearly, but we return to this point at the end of this subsection. We will tune L_t such that $k_{F_x}^2$ is of the same order of magnitude as the gap energy Δ, in which regime the Andreev approximation (22) is not valid, and call such a L_t value a critical width.

Figures 3 and 4 show the results for a configuration in which $(n_y, n_z) = (2,2)$ is the highest allowed mode. The chemical potentials in the superconductor and in the normal metal μ_S and μ_N, respectively, are assumed equal with magnitude 0.5. The longitudinal dimension L of the normal-metal part is 4000 Bohr and the gap Δ is treated as real with magnitude 0.0001 Ry. The LDOS in the normal-metal part at $x = 1000$ Bohr is plotted against E/Δ. The peaks represent discrete energy states.[12] We make the width of the curves, determined by the parameter δ in $E + i\delta$, wide enough so that the fundamental features can be seen. The numbers in parentheses denote the mode to which the energy belongs. In Fig. 4 the transverse width is determined by the condition that $k_{F_x}^2 = \Delta$ for the mode (2,2), by which one finds that $L_t = 12.5676$ Bohr and in Fig. 3 the transverse width is $L_t = 13$ Bohr. Although the latter width is slightly larger than the critical width and has the same allowed modes, the corresponding $k_{F_x}^2 = 328\Delta$. Clearly for the latter value the Andreev approximation (AA) is very good, which can be seen in Fig. 3. In both figures the dashed curve is the local density of states calculated using the AA and the solid curves are the results from the exact calculation. In Fig. 3, the exact and the AA results coincide and just three states are found, one for each mode. For the critical width, the states for the first two modes are at almost the same position, but for the (2,2) mode many states are found. The AA clearly breaks down, merely showing some average of the location of the exact peaks. Further we notice that the AA peaks have about the same height whereas the amplitudes of the exact peaks vary widely with the energy. The amplitude variation of the exact peaks is due to the specific position chosen for the LDOS. Figure 5 depicts the exact LDOS at $x = 1000$ and 1500 Bohr. We observe that some of the peaks in the solid curve are suppressed while the corresponding peaks in the dashed curve are prominent and vice versa. The suppressed peaks are pulled down by the small magnitude of the weighting wave functions at those values of x. The degenerate traveling waves corresponding to the AA are split in the exact treatment into odd and even (sine and cosine) functions having different heights at different positions.[17]

In general, critical widths are determined by the condition $0 < k_{F_x}^2 \approx \Delta$. It is clear that the number of peaks for the highest mode will increase for smaller values of $k_{F_x}^2$ compared to the value used in Fig. 4. For larger values the effects will diminish. We will not expand on this obvious detail.

Finally, we want to comment on our choice of the transverse width up to now. In Sec. IV it will come out that superconductivity is suppressed for transverse widths in the order of 20 Bohr or less. This means that so far our choice of

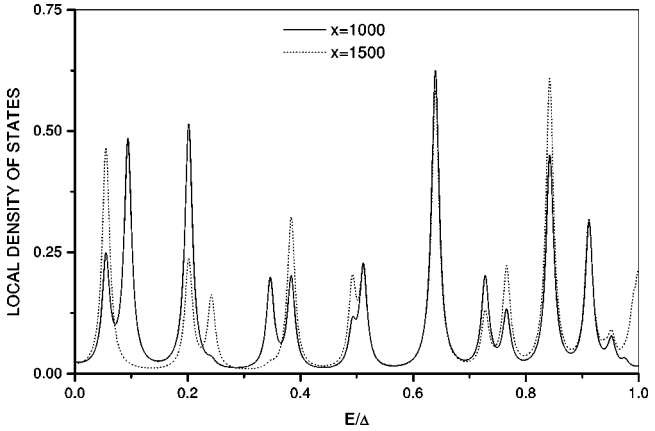

FIG. 5. Plot of the LDOS for a *SNS* system against E/Δ at $x=1000$ Bohr (solid curve) and $x=1500$ Bohr (dashed curve). The transverse dimension is $L_t=12.5676$ Bohr and the length of the normal metal is $L=4000$ Bohr.

transverse widths may seem not too appropriate. We chose those transverse widths to illustrate with clarity the fundamental features of the bound states. In order to see the influence of a wider transverse dimension, we show in Fig. 6 the LDOS of a *SNS* system with $L_t=100$ Bohr (solid curve) and $L_t=99.8514$ Bohr (dotted curve). The critical transverse width of 99.8514 Bohr is obtained from the condition $k_{F_x}^2=\Delta$ for the mode (19, 12). To illustrate its main features clearly, we only show the results for the Andreev approximation. It appears that higher modes are allowed for a wider transverse dimension. The peak at about $E=0.95\Delta$ comes from the many lower modes, each supporting just one bound state. Only the highest mode gives rise to the distinct set of peaks starting at about $E=0.074\Delta$. So effectively, the character of the results shown above is essentially unchanged.

B. The *SNSNS* system

A schematic representation of the system is shown in the lower panel of Fig. 1. The height of the middle superconductor is chosen to take the values $h\Delta$ where the range of h is $0\leqslant h\leqslant 1$. The LDOS is calculated using Eq. (23). The process of determining the t matrix, the T matrix, and the Green's function for the *SNSNS* junction is the same as in the *SNS* junction. The number of interfaces has increased by 2, and the dimension of the matrices has become 16 instead of 8. We again choose a square transverse cross section whose dimension is $L_t=12.5676$ Bohr. This means that the set of modes is the same as in the *SNS* system. The lengths of the normal metal parts are each 1000 Bohr and that of the middle superconductor is 2000 Bohr.

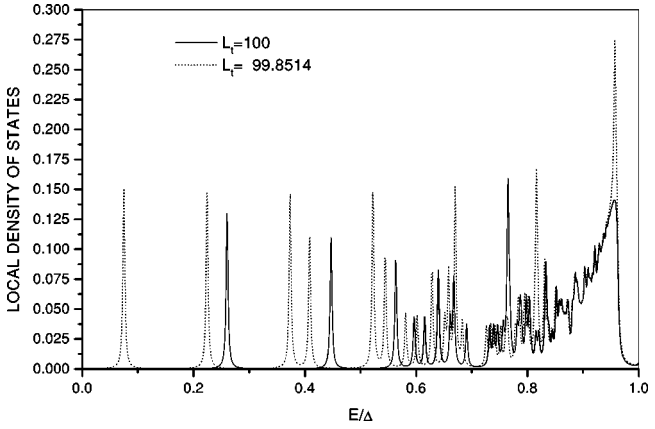

FIG. 6. Plot of the LDOS against E/Δ for a *SNS* system in which $L_t=100$ Bohr (solid curve) and $L_t=99.8514$ Bohr (solid curve). The length of the normal-metal part is 4000 Bohr.

Figure 7 shows the development of the bound states as the gap of the middle superconductor is increased from 0.25Δ to Δ. All peaks belong to the highest (2,2) mode, apart from a (1, 1) mode and a (1, 2) mode peaks just below $E/\Delta=1$. The mode labels are shown only in Fig. 7(d) to avoid cluttering the figures. Both the exact solution and the states according to the Andreev approximation (AA) are shown. Again the lifting of degeneracy is observed in the exact results. The distribution of the peak heights shown corresponds to a calculation of the LDOS at $x=-1500$ Bohr. Results for other positions just give other distributions of peak heights. From now on, we concentrate on the position of the AA peaks to facilitate the comparison of the different figures. The *SNSNS* system with $h=0$ is equivalent to the *SNS* system, so it is interesting to compare Fig. 4 with Figs. 7(a)–7(d). One can see a general shift of the states in the latter figure to the right relative to the states in Fig. 4. For the system with $h=0.25$ the $h=0$ state at $E=0.075\Delta$ suffers a large displacement. This can be understood as follows. States below $E=0.25\Delta$ see a longitudinal length L_N of 1000 Bohr whereas the states above $E=0.25\Delta$ see a length L_N of 4000 Bohr, L_N being the length of the N metal. According to a quasiclassical result,[6,10] bound-state energies scale as v_F/L_N, so they are inversely proportional to the longitudinal length, which would imply a shift upwards to $E=0.3\Delta$. However, the separation of 2000 Bohr between the N parts is smaller than the BCS coherence length $v_F/\pi\Delta\approx 4500$ Bohr, which suggests that the N parts of the system are not completely decoupled yet. This is the reason why the lowest state is found below $E=0.25\Delta$, namely at $E=0.19\Delta$. The positions of the other peaks are hardly changed.

Looking at Figs. 7(b)–7(d) one sees that the lowest state stabilizes at a position of about $E=0.26\Delta$. All other states are shifted more and more upwards for increasing h values. For $h=0.5$, Fig. 7(b), still a set of peaks is found above 0.5Δ, in Fig. 7(c) the set starts at about $E=0.75\Delta$. For $h=1$, Fig. 7(d), only three states are seen just below $E=\Delta$, apart from a state at $E=0.78\Delta$, lying three times as high as the lowest state, in agreement with the quasiclassical picture. A test calculation for a *SNS* system with $L_N=1000$ Bohr differs from Fig. 7(d) only as far as the position of the highest peak, the (1, 1) peak, is concerned.

The idea of decoupling can also be illustrated by Fig. 8. For the sake of clarity we just give the results for the Andreev approximation. Figure 8(a) shows the LDOS for a *SNSNS* system with $L=6000$ Bohr. The lengths of the N parts are kept at 1000 Bohr but now the length of the middle superconductor is 4000 Bohr, slightly below the BCS coherence length of approximately 4500 Bohr. In Fig. 8(b), the

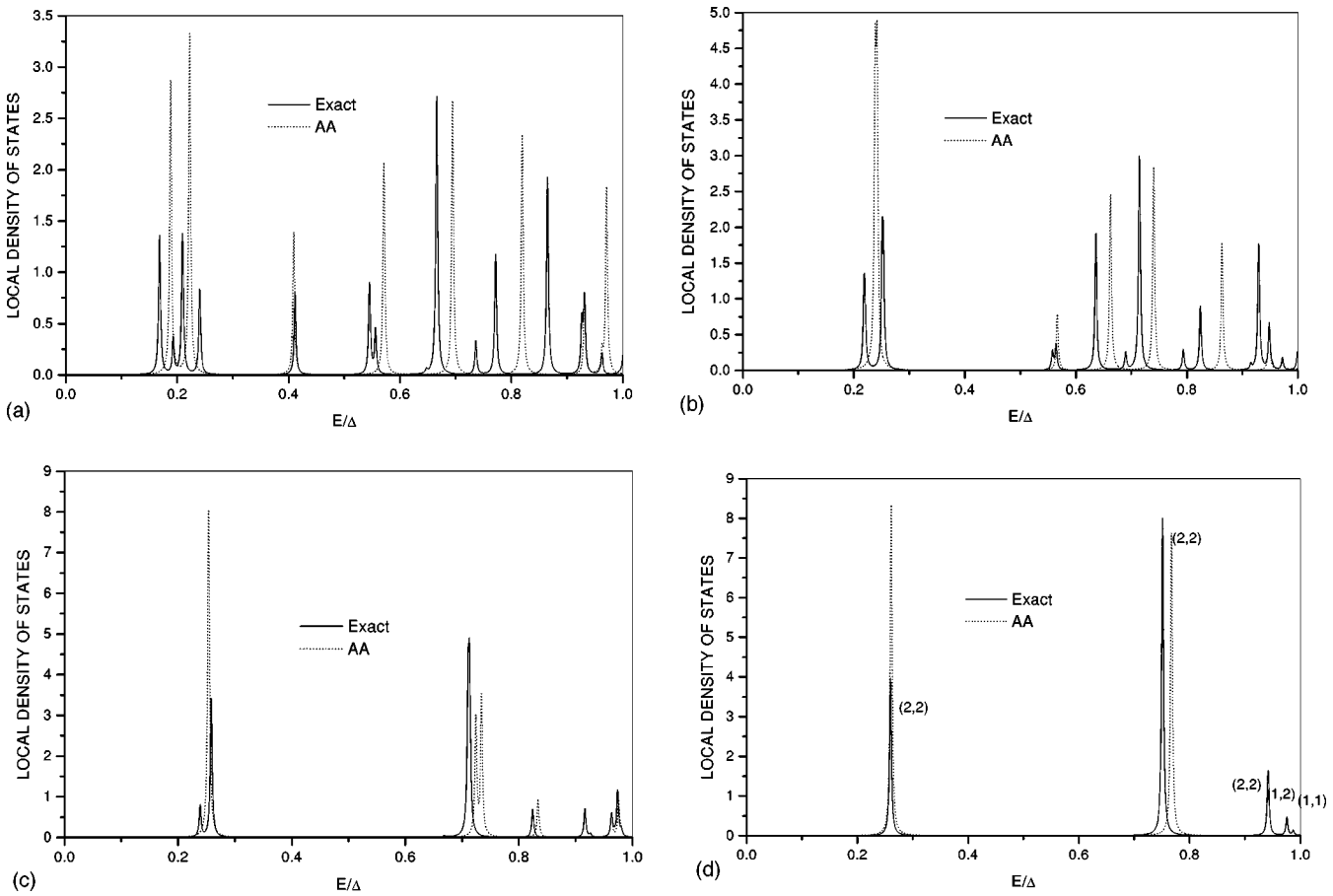

FIG. 7. Plot of the LDOS at $x=-1500$ Bohr against E/Δ for a *SNSNS* system in which $L_t=12.5676$ Bohr for (a) $h=0.25$, (b) $h=0.5$, (c) $h=0.75$, and (d) $h=1$.

length L of the *SNSNS* system is 8000 Bohr and the lengths of the N parts are again kept at 1000 Bohr. This makes the middle superconductor 6000 Bohr in length, which is longer than the BCS coherence length. In both figures the gap of the middle superconductor is 0.25Δ. Thus, there is effectively complete decoupling in Fig. 8(b). In addition, one sees that the (2, 2) peaks are lying closer to one another for the longer system, which is in line with the V_F/L_N behavior of the energies.

IV. SELF-CONSISTENT CALCULATION OF THE GAP

In the preceding discussions, the gap function Δ used in the calculation is steplike, that is, it has a finite constant value in the superconducting part and is zero in the normal part. At the interfaces, it has a step discontinuity. This configuration is shown in Fig. 1. So in the calculation of the bound states in Sec. III, the proximity effect is not taken into account. However, we want to demonstrate in this section that our formalism makes it possible to show that the actual gap function is not steplike, but decreases smoothly towards the interface and abruptly goes down to zero in the normal metallic layer. This proximity effect is studied in the present section. In addition, the actual gap function will be calculated self-consistently.

The self-consistency condition is given by

$$\Delta(x)=-VF(\mathbf{r},\mathbf{r},0^+) \tag{27}$$

in which $F(\mathbf{r},\mathbf{r},0^+)$ is the well-known anomalous Green's function[19] given by the upper right element of the original ($\mathbf{r}$, τ)-dependent matrix Green's function. Taking into account the expansion of the matrix Green's function over the Matsubara frequencies and the transverse wave vectors, we obtain

$$\Delta(x)=-\frac{V}{\beta L_y L_z}\sum_{\omega_n,k_y,k_z} F(x,x,k_y,k_z,i\omega_n), \tag{28}$$

where $F(x,x,k_y,k_z,i\omega_n)$ is the upper right element of the matrix Green's function in Eq. (20). The summation over the Matsubara frequencies is restricted by the Debye temperature θ_D according to the formula

$$k_B\theta_D=\omega_{n_{\max}}=n_{\max}\pi k_B T. \tag{29}$$

The summation over the transverse wave vector is over all positive values of k_y and k_z according to Eq. (3). Evaluation of the summation takes much computer time, so we resort to some approximations. Since the cross section is a square, that is $L_y=L_z$, an excellent approximation to reduce the number of terms is to partition the transverse $k_\perp$ plane by concentric circles with radius $k_\perp=\sqrt{k_y^2+k_z^2}$ and a $\delta k_\perp=\pi/L_t$. The number of allowed values of k_y and k_z in each

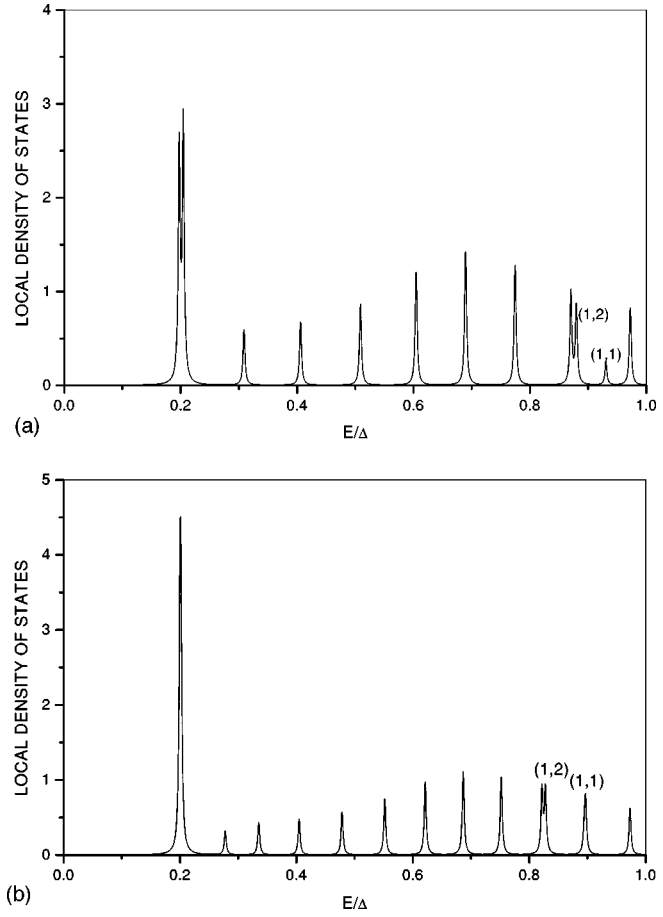

FIG. 8. The LDOS against E/Δ for a *SNSNS* system in which $L_t = 12.5676$ Bohr. In (a) $L = 6000$ Bohr, the length of the middle superconductor is 4000 Bohr and the LDOS is calculated at $x = -2500$ Bohr. In (b) $L = 8000$ Bohr, the length of the middle superconductor is 6000 Bohr and the LDOS is calculated at $x = -3500$ Bohr. The gap of the middle superconductor is 0.25Δ. All unlabeled LDOS peaks belong to the mode (2, 2). The calculation is done in the Andreev approximation.

ring is given by its surface divided by the density of the transverse k states $(\pi/L_t)^2$. Another approximation can be made by noting that the terms involving $k_\perp \gg \sqrt{\mu}$ do not have significant contributions to the sum. This allows us to evaluate a finite number of terms instead of evaluating an infinite series. In our calculation we take $k_{\perp\,\max} = 3\sqrt{\mu}$. In determining the coupling constant V according to the BCS relation

$$T_c = 1.13\omega_D e^{-1/N(\mu)}, \quad \text{with} \quad N(\mu) = \frac{\mu}{4\pi^2} \tag{30}$$

we use $T_c = 1.2$ K and $\omega_D = 375$ K for aluminum. We find $V = 9.516$ Ry.

A. The bar-shaped superconductor

The matrix Green's function for a bar-shaped superconductor $G_S^0(x,x,k_y,k_z,i\omega_n)$ is given by Eq. (14). By substituting the upper right element of this Green's function in Eq. (28) one straightforwardly obtains the following selfconsistency condition for the homogeneous bar-shaped superconductor

$$\Delta(x) = \frac{V|\Delta|}{\beta L_y L_z} \sum_{\omega_n,k_y,k_z} \frac{1}{4\Omega_S}\left(\frac{1}{\sqrt{k_{F_x}^2 + i\Omega_S}} + \frac{1}{\sqrt{k_{F_x}^2 - i\Omega_S}}\right). \tag{31}$$

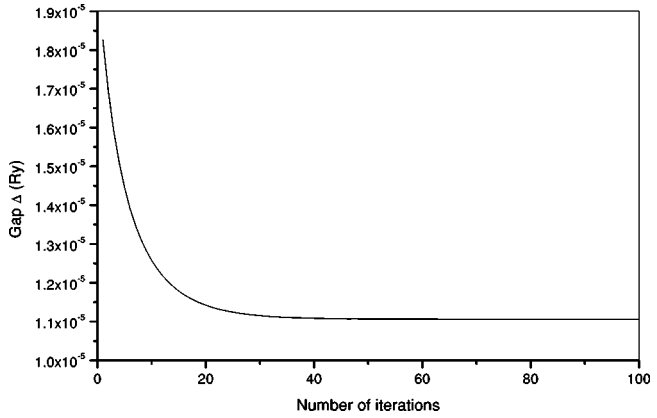

FIG. 9. The gap against the number of iterations for a bar-shaped superconductor. Note that the value of the gap stabilizes as the number of iterations increases. For the system considered, $L_t = 1000$ Bohr and $T = 0.6$ K.

In calculating the gap self-consistently, we first assume an initial value of the gap. By substituting it on the right-hand side of Eq. (31) we obtain a new value of the gap. Then this new value is again substituted on the right-hand side to get another new value. This procedure can be repeated until the difference between successive iterations is negligibly small. As shown in Fig. 9, the difference between the first ten iterations is still significant. After about 80 iterations, the value of the gap stabilizes to 1.106×10^{-5} Ry. The transverse length is 1000 Bohr and the temperature is 0.6 K. The initial value of the gap is 2.0×10^{-5} Ry.

Figure 10 shows the plot of the gap against the transverse length L_t for different temperatures. The number of iterations

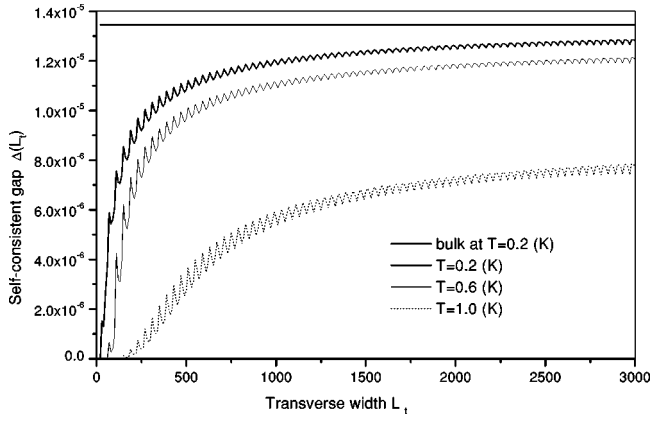

FIG. 10. Plot of the self-consistent gap function against the transverse length L_t for a bar-shaped superconductor at different temperatures. The number of iterations is 100.

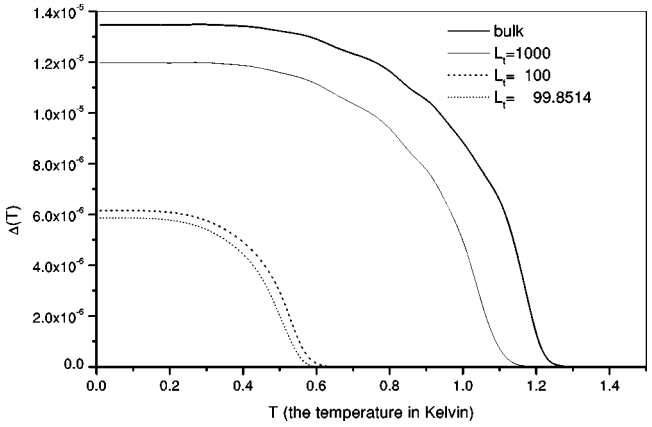

FIG. 11. The temperature variation of the self-consistent gap for different transverse widths.

is 100. It can be seen that there are oscillations of the gap. The amplitudes of the oscillations decrease as the transverse dimension increases. These oscillations can be attributed to the discreteness of the transverse wave vector. As the transverse width increases, the transverse wave vector approaches the continuous regime which can be gauged from the gap becoming closer to its bulk value obtained by integrating instead of summing over the transverse wave vectors. In the figure, we show the bulk value at 0.2 K. Another interesting thing which can be seen in the figure is the suppression of superconductivity for narrower transverse dimensions. We notice that as the temperature increases the onset of the suppression of superconductivity occurs at higher values of L_t.

In Fig. 11 we show the temperature variation of the gap for different transverse widths L_t. A residual value of the gap for the bulk superconductor can still be observed beyond the critical temperature (1.2 K for aluminum). We also notice small-amplitude oscillations of the gap at higher temperatures, which only show up in the curves for larger transverse dimensions. For smaller transverse dimensions, the oscillations are suppressed. These oscillations are due to the cutoff in the summation over the Matsubara frequencies. For lower temperatures, the cutoff value $n_{\max}$ in Eq. (29) becomes very large and the results are no longer sensitive to it.

B. The *NS* system

The matrix Green's function appropriate for a normal metal-superconductor system is given in Eqs. (16) and (17). The first term on the right-hand side of Eq. (16) is the matrix Green's function for the bar superconductor. The second term contains the elements of the t matrix, which take into account the scattering of the quasiparticles at the interface. The latter acts as a perturbing term to the former and is therefore responsible for the spatial variations of the gap and the pair amplitude at the vicinity of the interface. To calculate the spatial variation of the gap according to Eq. (28), we substitute the upper right element of the matrix Green's function, Eq. (16), using the value of the self-consistent gap for the bar-shaped superconductor.

Before presenting our results, we want to mention a computational problem which has to be solved. Due to the explicit presence of the position x_j in Eq. (18), the matrices involved have alternating columns of very small and very large values which the computer cannot handle anymore. However, this problem is not intrinsic to the formalism and can be solved by appropriate rescaling. By defining the matrix $\hat{t}$

$$\hat{t}^{\sigma\sigma'\nu\nu'}_{\nu j\nu' j} \equiv e^{i\sigma\nu k^{\sigma}_{\nu j} x_j} t^{\sigma\sigma'\nu\nu'}_{\nu j\nu' j} e^{i\sigma'\nu' k^{\sigma'}_{\nu' j} x_j} \tag{32}$$

the Green's function (16), combined with Eq. (17), obtains the form

$$\begin{aligned} G_{\nu j\nu' j}(x,x',k_y,k_z,i\omega_n) &= \sum_{\sigma} d^{\sigma}_{\nu j}\psi^{\sigma\mu}_{\nu j}(x)\tilde{\psi}^{\sigma,-\mu}_{\nu j}(x')\delta_{\nu\nu'} \\ &+ \sum_{\sigma\sigma'} d^{\sigma}_{\nu j} d^{\sigma'}_{\nu' j'} \psi^{\sigma\nu}_{\nu j}(x-x_j)\hat{t}^{\sigma\sigma'\nu\nu'}_{\nu j\nu' j}\tilde{\psi}^{\sigma'\nu'}_{\nu' j}(x'-x_j) \end{aligned} \tag{33}$$

in which only position differences occur. The rescaled matrix $\hat{t}$ is determined by the equation

$$\sum_{\sigma\nu} \nu d^{\sigma}_{\nu j}\psi^{\sigma\nu}_{\nu j}(0)\hat{t}^{\sigma\sigma'\nu\nu'}_{\nu j\nu' j} = -\nu'\psi^{\sigma',-\nu'}_{\nu' j}(0), \tag{34}$$

found straightforwardly from the original equation (18).

Figure 12(a) shows the spatial variation of the gap near the interface of a normal metal-superconductor system at $T=0.6$ K for different transverse widths. At a distance of 30 000 Bohr from the interface, which is about six times the coherence length ($\approx$4500 Bohr), the gap is slightly smaller than the one obtained for the bar-shaped superconductor. The differences are about 7.79, 6.57, and 2.93 % of their bar value for $L_t=99.8514$, $L_t=100$, and 1000 Bohr, respectively. At 4000 Bohr, which is of the order of the coherence length from the interface, the differences are about 21.7, 20.44, and 14.71 %, respectively. These figures lead to the inevitable conclusion that for larger transverse dimensions, the proximity effect is less pronounced than for smaller ones. This may be due to the fact that for small transverse dimensions the superconductivity tends to be suppressed. We find that the difference seen for the two smaller widths can be attributed to the oscillations in the self-consistent gap shown in Fig. 10. We have not seen a special influence of the fact that the smaller width is a critical one. Figure 12(b) shows the corresponding pair amplitude defined by $\Delta(x)/V$ [see Eq. (27)] which has a finite value in the normal metallic region near the NS interface but it decays in the inner region of the normal metal.

C. The *SNS* system

In the superconductor-normal metal-superconductor system, there are two interfaces which we designate as x_1 and x_2. The t matrices must be determined at these interfaces so that we can evaluate the T matrix. The unpleasant singularities due to the explicit presence of the position of the inter-

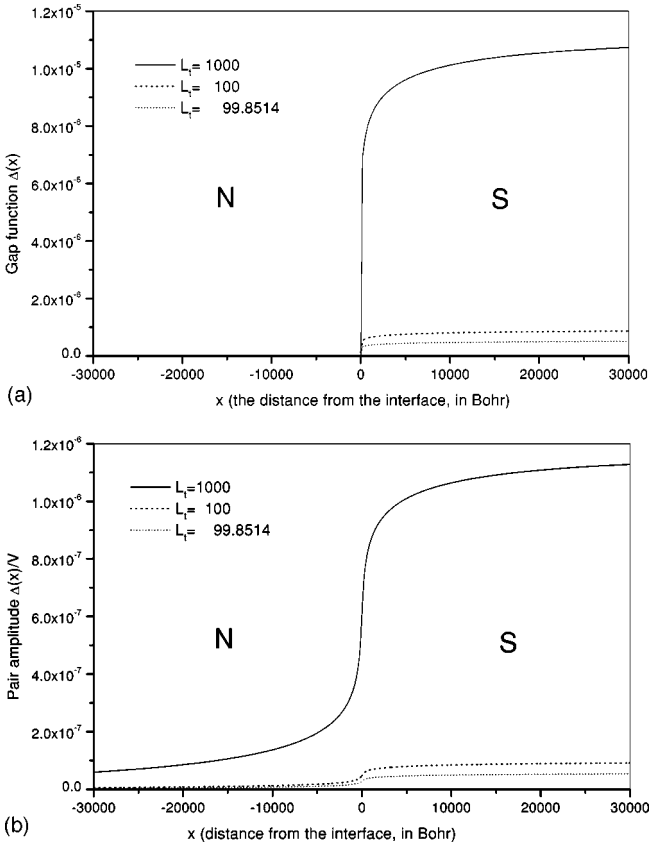

FIG. 12. (a) The gap and (b) the pair amplitude against the distance from the interface of a *NS* system at $T=0.6$ K. The interface is chosen at $x=0$.

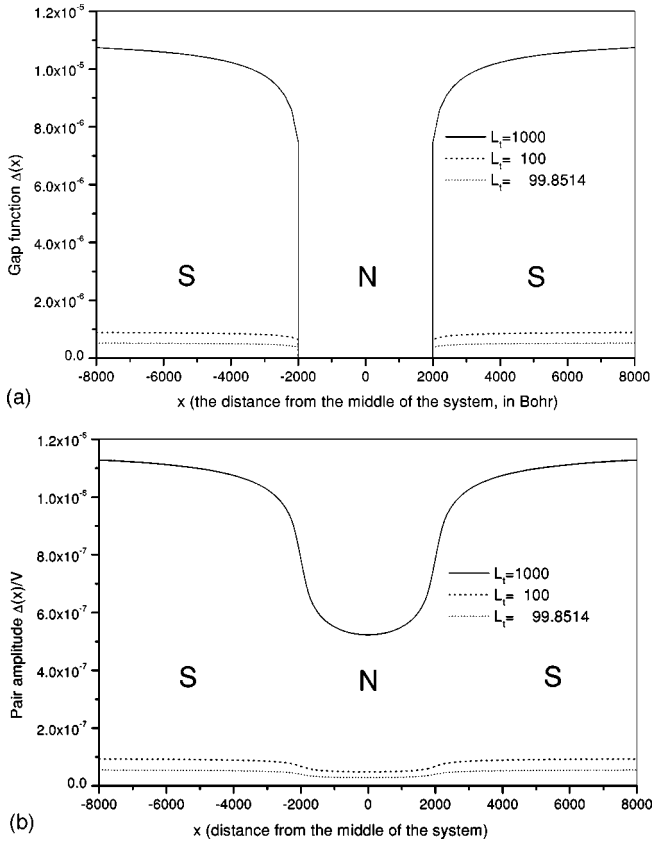

FIG. 13. (a) The gap function and (b) the pair amplitude of a *SNS* system against the distance from the middle of the system chosen at $x=0$. The interfaces are located at $x=\pm 2000$.

faces in Eq. (18) can be removed by using Eq. (32) resulting to a corresponding transformation of the T matrix given by

$$\hat{T}^{\sigma\sigma'\nu\nu'}_{\nu j\nu' j'} = e^{i\sigma\nu k^{\sigma}_{\nu j} x_j} T^{\sigma\sigma'\nu\nu'}_{\nu j\nu' j'} e^{i\sigma'\nu' k^{\sigma'}_{\nu' j'} x_{j'}}. \tag{35}$$

By implementing this, the multiple-scattering Green's function (20) and Eq. (21), which determines the T matrix in terms of the t matrices, can be modified straightforwardly.

The steps in calculating the gap and the pair amplitude self-consistently are the same as in Sec. IV B. Figure 13 shows the self-consistent gap function and the pair amplitude for different transverse widths. The center of the system is at $x=0$. The spatial variation of the gap near the interfaces is clearly shown. The proximity effect is stronger than for the *NS* system shown in Fig. 12. Whereas in Fig. 12(a) for $L_t = 1000$ Bohr the gap at a distance of 6000 Bohr from the interface has a value of 9.753×10^{-6} Ry, in Fig. 13(a) it has already increased to 1.074×10^{-5} Ry, which is much closer to the bulk value of 1.106×10^{-5} Ry. In Fig. 13(b) the pair amplitude in the *N* region does not decrease below a value of 5×10^{-7}. In Fig. 12(b) it decreases to zero and the value at 2000 Bohr from the *NS* interface has already decreased to 2.784×10^{-7}. In Fig. 14 we show the gap functions for different values of L. It can be seen that for larger L the gap function is lesser in magnitude. This is another manifestation of the proximity effect.

D. The *SNSNS* system

The extension of the steps outlined in Sec. IV C leading to the T matrix and the matrix Green's function for a *SNSNS* system is straightforward. In this case we have to consider four interfaces but the procedure is basically the same. In the outer superconductors, we again use the self-consistent value of the gap for the superconducting bar we have calculated in

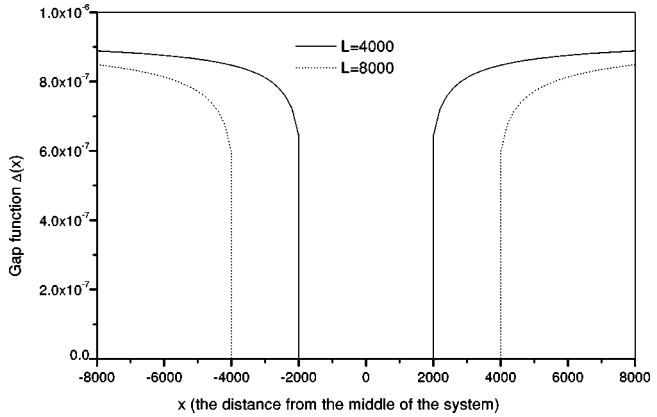

FIG. 14. The gap function of a *SNS* system against the distance from the middle of the system chosen at $x=0$ for different values of L. The interfaces are located at ± 2000 for $L=4000$ Bohr and at ± 4000 for $L=8000$ Bohr.

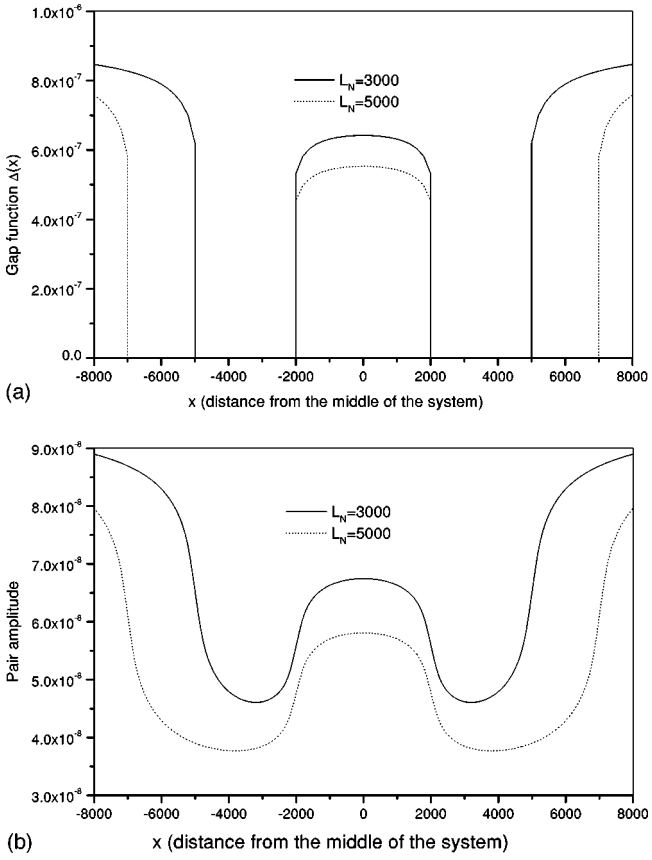

FIG. 15. (a) The gap function and (b) the pair amplitude against the distance from the middle of a *SNSNS* system, which is chosen at $x=0$. The interfaces are chosen at $x=\pm 2000, \pm 5000$ for $L_N=3000$ Bohr (solid curve) and $x=\pm 2000, \pm 7000$ for $L_N=5000$ Bohr (dotted curve). The transverse width is $L_t=100$ Bohr.

Sec. IV A. In calculating the gap in the middle superconductor self-consistently, we apply the recipe introduced by Tanaka and Tsukada.[13] We start the iteration procedure by taking half of the gap in the outer superconductors for the gap in the middle. By substituting these values in the right-hand side of Eq. (28), the middle x-dependent gap function is obtained and its spatial average is determined. This average value is used as the new value of the gap in the middle superconductor. The process is repeated until the difference of these average values between successive iterations is negligibly small. To determine the gap's spatial variation, the self-consistent average value of the gap in the middle superconductor and the bar value in the outer ones are substituted in the right-hand side of Eq. (28).

Figure 15 shows the gap and the pair amplitude of two *SNSNS* systems, one with a length $L_N=3000$ Bohr for the normal metallic parts and the other one with a larger length $L_N=5000$ Bohr. First note that the gap of the middle superconductor is smaller than the gap of the outer superconductors although the metallic parameters for these superconductors are taken equal. This supports our choice of a h value smaller than 1 in Sec. III, see Fig. 1. Further note that the gap and the pair amplitude are higher for the system with narrower normal-metal part, which is just another manifestation of the proximity effect. Although by definition the gap is zero in the normal-metal parts, the pair amplitude is different from zero. This is also a manifestation of the proximity effect. If the width of the normal-metal layers had been much larger than the sum of the coherence lengths of the outer and middle superconductors, the pair amplitude would have been zero there except in those regions near the interfaces.

V. CONCLUSIONS AND FUTURE PROSPECTS

The multiple-scattering Green's function formalism developed by Koperdraad[18] has been applied to determine the Andreev bound states in *SNS* and *SNSNS* junctions through the local density of states and to calculate the superconducting gap function self-consistently. We have shown that for transverse junction widths tuned such that the motion in the longitudinal direction is very slow, the Andreev approximation breaks down. For these transverse dimensions, the highest mode is supported by many bound states whose degeneracy is lifted when no approximation is applied. The thickness used for the normal metallic layers is chosen such that the lower modes are each supported by only one nondegenerate state. Results for the self-consistent gap functions exhibit various features of the proximity effect. Furthermore, our results show that for small transverse dimensions, superconductivity is suppressed.

The formalism is applicable to systems of an arbitrary number of layers. In addition, it allows for the calculation of the supercurrents through such junctions, to which self-consistent gap functions are necessary.[13,18] This will be investigated in the near future.

ACKNOWLEDGMENTS

The stay of one of us (R.E.S.O.) at the Vrije Universiteit Amsterdam was made possible by the Netherlands University Foundation for International Cooperation (NUFFIC) through support of the Physics Development Project of the University of San Carlos in Cebu, The Philippines, a cooperation of the University of San Carlos and the Vrije Universiteit Amsterdam.

*On leave from the University of San Carlos, Nasipit, Talamban, Cebu City, Philippines.
†Corresponding author. E-mail address: alod@nat.vu.nl

[1] A. F. Andreev, Sov. Phys. JETP **19**, 1228 (1964); **24**, 1019 (1967).
[2] E. Scheer, W. Belzig, Y. Naveh, M. H. Devoret, D. Esteve, and C. Urbina, Phys. Rev. Lett. **86**, 284 (2001).
[3] P. Dubos, H. Courtois, B. Pannetier, F. K. Wilhelm, A. D. Zaikin, and G. Schön, Phys. Rev. B **63**, 064502 (2001).
[4] N. M. Chtchelkatchev, G. B. Lesovik, and G. Blatter, Phys. Rev. B **62**, 3559 (2000).
[5] J. A. Melsen, P. W. Brouwer, K. M. Frahm, and C. W. J. Beenakker, Phys. Scr. **T69**, 223 (1997).
[6] A. Lodder and Yu. V. Nazarov, Phys. Rev. B **58**, 5783 (1998).
[7] See *Mesoscopic Superconductivity*, edited by P. F. Bagwell, Su-

perlattice Microstruct. **25,** 6 (1999).
[8] K. D. Usadel, Phys. Rev. Lett. **25**, 507 (1970).
[9] G. Kieselmann, Phys. Rev. B **35**, 6762 (1987).
[10] M. Ashida, S. Aoyama, J. Hara, and K. Nagai, Phys. Rev. B **40**, 8673 (1989).
[11] A. I. Larkin and Yu. V. Ovchinninkov, Sov. Phys. JETP **41**, 960 (1975).
[12] M. Blaauboer, R. T. W. Koperdraad, A. Lodder, and D. Lenstra, Phys. Rev. B **54**, 4283 (1996).
[13] Y. Tanaka and M. Tsukada, Phys. Rev. B **44**, 7578 (1991).
[14] B. P. Stojkovic and O. T. Valls, Phys. Rev. B **50**, 3374 (1994).
[15] P. Miller and J. K. Freericks, J. Phys.: Condens. Matter **13**, 3187 (2001).
[16] R. Kümmel, Phys. Rev. B **10**, 2812 (1974).
[17] O. Šipr and B. L. Györffy, J. Phys.: Condens. Matter **8**, 169 (1996), and references therein.
[18] R. T. W. Koperdraad, R. E. S. Otadoy, M. Blaauboer, and A. Lodder, J. Phys.: Condens. Matter **13**, 8707 (2001).
[19] L. P. Gor'kov, Sov. Phys. JETP **9**, 1364 (1959).
[20] C. Ishii, Prog. Theor. Phys. **44**, 1525 (1970).
[21] An equivalent but less flexible form has already been given by Ishii (Ref. 20), in his Eqs. (2.12a)–(2.12c). Similarly, our Green's function equation (12) is equivalent to his Eq. (2.7) and to Eq. (2.12) of Tanaka and Tsukada (Ref. 13), but Ishii's approach towards a solution lies closer to our approach.